

In vivo evaluation of riboflavin receptor targeted fluorescent USPIO in mice with prostate cancer xenografts

Jabadurai Jayapaul^{1,2,3} (✉), Susanne Arns¹, Matt Bunker^{4,5}, Marek Weiler¹, Sandra Rutherford⁵, Peter Comba², and Fabian Kiessling¹ (✉)

¹ Institute for Experimental Molecular Imaging, RWTH Aachen University, Pauwelsstrasse 30, Aachen 52074, Germany

² Anorganisch-Chemisches Institut, Universität Heidelberg, Im Neuenheimer Feld 270, Heidelberg 69120, Germany

³ Molecular Imaging Group, Department of Structural Biology, Leibniz Institut für Molekulare Pharmakologie (FMP), Robert-Rössle-Str. 10, Berlin 13125, Germany

⁴ AstraZeneca, Pharmaceutical Development, Charter Way, Macclesfield, Cheshire SK10 2NA, UK

⁵ Molecular Profiles Ltd., 8 Orchard Place, Nottingham Business Park, Nottingham NG8 6PX, UK

Received: 30 October 2015

Revised: 21 January 2016

Accepted: 24 January 2016

© The author(s) 2016. This article is published with open access at Springerlink.com

KEYWORDS

flavin mononucleotide, iron oxide nanoparticles, magnetic resonance imaging, molecular imaging, riboflavin carrier protein, riboflavin transporters

ABSTRACT

Riboflavin (Rf) receptors bind and translocate Rf and its phosphorylated forms (e.g. flavin mononucleotide, FMN) into cells where they mediate various cellular metabolic pathways. Previously, we showed that FMN-coated ultrasmall superparamagnetic iron oxide (FLUSPIO) nanoparticles are suitable for labeling metabolically active cancer and endothelial cells *in vitro*. In this study, we focused on the *in vivo* application of FLUSPIO using prostate cancer xenografts. Size, charge, and chemical composition of FLUSPIO were evaluated. We explored the *in vitro* specificity of FLUSPIO for its cellular receptors using magnetic resonance imaging (MRI) and Prussian blue staining. Competitive binding experiments were performed *in vivo* by injecting free FMN in excess. Bio-distribution of FLUSPIO was determined by estimating iron content in organs and tumors using a colorimetric assay. AFM analysis and zeta potential measurements revealed a particulate morphology approximately 20–40 nm in size and a negative zeta potential (-24.23 ± 0.15 mV) in water. X-ray photoelectron spectroscopy and time-of-flight secondary ion mass spectrometry data confirmed FMN present on the USPIO nanoparticle surface. FLUSPIO uptake in prostate cancer cells and human umbilical vein endothelial cells was significantly higher than that of control USPIO, while addition of excess of free FMN reduced accumulation. Similarly, *in vivo* MRI and histology showed specific FLUSPIO uptake by prostate cancer cells, tumor endothelial cells, and tumor-associated macrophages. Besides prominent tumor accumulation, FLUSPIO accumulated in the liver, spleen, lung, and skin. Hence, our data strengthen our hypothesis that targeting riboflavin receptors is an efficient approach to accumulate nanomedicines in tumors opening perspectives for the development of diagnostic and therapeutic systems.

Address correspondence to Jabadurai Jayapaul, jayapaul@fmp-berlin.de; Fabian Kiessling, fkiessling@ukaachen.de

1 Introduction

Vitamins have been studied in the context of diagnostic and therapeutic agents because they are biocompatible, endogenously accessible, act as carriers, strongly bind to respective receptors, and mediate important cellular metabolic functions [1–3]. Their pivotal role in the prevention and treatment of different types of cancer has been explored in various clinical trials, thus promoting the development of vitamin-based drugs and imaging agents [4, 5]. In this context, a rapid translocation of the vitamin-tagged cargo into cancer cells was observed via receptor-mediated endocytosis, e.g. for folic acid- and riboflavin (Rf)-tagged agents [6–12]. In this study, we focused on Rf, an essential vitamin that mediates various biochemical, physiological, and metabolic (e.g. lipid, carbohydrate) functions in cells [13]. Interestingly, cells internalize Rf either as flavin mononucleotide (FMN) or flavin adenine dinucleotide (FAD), both of which, are vital sources of electrons required to facilitate redox reactions linked to different metabolic processes [14]. In the plasma and the extracellular space, Rf and its metabolic analogues (FMN/FAD) bind to a specific carrier protein, Rf carrier protein (RCP), shown to be highly expressed on the cell surface of metabolically active cells (e.g. prostate cancer cells and activated endothelial cells) [15]. Rf and the Rf-RCP complex are quickly internalised by cells via Rf transporters (RFTs). The rapid and efficient, clathrin-mediated endocytosis pathway plays a pivotal role in this process [16].

The biological significance of Rf led us to believe that its metabolic analogue, FMN could protect ultrasmall superparamagnetic iron oxide (USPIO) nanoparticles against oxidative degradation via a fluorescent adsorptive coating. Therefore, we designed RCP-targeted, fluorescent USPIO (FLUSPIO) as a contrast agent for magnetic resonance imaging (MRI) and demonstrated its ability to label metabolically active cancer cells as well as activated endothelial cells [17]. In another previous study, we developed a second MRI probe, FAD-USPIO, to assess vascular metabolism in prostate tumors [18]. Despite the development of these Rf-targeted molecular MRI probes, several uncertainties remain, regarding their performance *in vivo*, such as physiological stability (e.g. particle-protein

interactions), specificity of accumulation, binding to tumor and stroma cells, as well as bio-distribution.

Therefore, in addition to extended physicochemical characterization, we focused on the *in vivo* application of FLUSPIO in this study. We investigated the colloidal stability in physiological media, plasma protein adsorption, bio-distribution and accumulation of FLUSPIO in prostate cancer xenografts.

2 Experimental

2.1 Materials

Ferric chloride (FeCl_3 , >97%), ferrous chloride tetrahydrate ($\text{FeCl}_2 \cdot 4\text{H}_2\text{O}$ >99%), riboflavin-5'-monophosphate sodium salt dihydrate (flavin mononucleotide; FMN, 73%–79% fluorometric), IDRANAL III® standard solution (EDTA-Na_2 , reagent for metal titration, 0.1 M), 5-sulfosalicylic acid dihydrate ($\geq 99\%$ for metal titration), 4,5-dihydroxy-1,3-benzenedisulfonic acid disodium salt monohydrate (Tiron®) indicator, and trypan blue solution for microscopy were obtained from Sigma Aldrich GmbH (Steinheim, Germany). Ammonia ($\text{NH}_3 \geq 25\%$), N-(2-Hydroxyethyl)piperazine-N'-(2-ethanesulfonic acid) (HEPES, $\geq 99.5\%$), hydrochloric acid (HCl, 37%), $\text{K}_4[\text{Fe}(\text{CN})_6]$, nuclear fast red, and hematoxylin and eosin were purchased from Carl Roth GmbH (Karlsruhe, Germany). Guanosine-5'-monophosphate disodium salt hydrate (GMP, 98%), gelatin (ph. Eur. powder), phosphate-buffered saline (PBS) (10× Dulbecco's powder) were procured from Applichem (Darmstadt, Germany). Feraspin XS® used in this study was provided as a gift sample by Miltenyi Biotech GmbH (Bergisch Gladbach, Germany). Feraheme® was obtained from AMAG Pharmaceuticals, Inc. (Waltham, MA, USA). All chemicals were used as received without any further purification.

2.2 Synthesis of iron oxide nanoparticles (Fe_3O_4)

USPIO nanoparticles were synthesized by co-precipitation of ferrous (Fe^{2+}) and ferric (Fe^{3+}) salts under aqueous alkaline conditions as previously described [17, 18]. Briefly, in a stoichiometric ratio of $2\text{Fe}^{3+}:\text{Fe}^{2+}$, 16 mmol (2.66 g) FeCl_3 and 8 mmol (1.63 g) $\text{FeCl}_2 \cdot 4\text{H}_2\text{O}$ dissolved in 190 mL de-ionized water were co-precipitated using 10 mL 25% NH_3 . The nanoparticles

were washed with water and 0.1 M HCl and stored under acidic conditions (pH 2) until further use. The total iron content (Fe^{3+} ions) of USPIO (161 mM) was determined by titrimetric [19] and colorimetric [20] methods.

2.3 Synthesis of FLUSPIO nanoparticles

FLUSPIO nanoparticles were prepared as previously described [17]. Briefly, 143 mM USPIO (pH 4) was sonicated with 35 mM FMN for 1 h at ambient temperature. Subsequently, the FMN-covered nanoparticles were washed with water under the influence of high-gradient magnetophoresis and then sonicated with 50 mM GMP for 1 h. After final coating and high-gradient magnetophoresis-assisted washing with water, the particles were stored at 4 °C until further use.

2.4 General characterization

2.4.1 Atomic force microscopy (AFM)

Samples for AFM analysis were prepared using FLUSPIO (5 μL) in water, which were deposited onto a polymer membrane (Nucleopore 0.1 μm , Whatman) that provided a flat surface to visualize the nanoparticles. Samples were dried in a fume hood for 1.5 h, which led to the formation of a ring of dried material at the perimeter of the dried droplet, providing a high concentration of particle aggregates as a target for AFM imaging.

All AFM images were captured in tapping mode on a multimode nanoscope IIIa instrument (Veeco, USA) using BudgetSensors Tap300 probes. Topographic and phase images were recorded simultaneously from the same area of sample.

2.4.2 Dynamic light scattering (DLS) measurements

The size distribution of USPIO and FLUSPIO in 10 mM HEPES buffer (pH 7.2) with different concentrations of human serum albumin (HSA) was investigated by DLS using the Malvern Zetasizer, Nano-S (Malvern, UK).

2.4.3 Zeta potential measurements

Zeta potential and electrophoretic mobility of USPIO and FLUSPIO were determined using a Malvern 4700 system (Malvern Ltd., Malvern, UK). Freshly prepared nanoparticles (0.5 mL) were diluted (1,000-fold) in

water, 5% (*w/v*) glucose solution, fetal calf serum (FCS), 1:1 (*v/v*) mixture of 5% glucose solution and FCS, or 25 mM HEPES buffer (pH 7.2), respectively. After dilution, each sample was measured on an average of seven runs (\pm the standard deviation) in triplicates. Intralipid was used as a reference for zeta potential measurements.

2.4.4 Fluorescence spectroscopy

The fluorescence spectra of FMN and FLUSPIO suspended in different physiologically relevant solutions (5% (*w/v*) glucose solution, FCS alone, and 1:1 (*v/v*) mixture of 5% glucose solution and FCS) were recorded for different fluorophore (FMN) and iron (FLUSPIO) concentrations ranging from 10^{-5} to 10^{-12} M (37 °C) using the TECAN Infinite M200pro (Tecan group, Maennedorf, Switzerland) plate reader.

2.4.5 Magnetic resonance (MR) relaxometry (phantom studies)

MR relaxometry of FLUSPIO and Feraspin XS[®] (Miltenyi Biotech, Germany), a preclinical MR contrast agent for visualizing vasculature, was performed using a clinical (3T) whole-body MR scanner (Philips Achieva, The Netherlands) in combination with a knee coil (SENSE-flex-M, Philips, The Netherlands) at room temperature. FLUSPIO and Feraspin XS[®] were diluted in de-ionized water at concentrations ranging from 0.005 to 50 μg Fe/mL. For MR measurements, 0.3 mL diluted FLUSPIO and Feraspin XS[®] solution was filled in custom-made phantoms. For T_2 relaxometry in phantoms, images were acquired at 20 echo times (TE range = 8–180 ms) using a multi-slice, multi-shot, spin-echo sequence (1,500 ms TR, 8.1 ms inter-echo spacing, 96×96 reconstruction matrix size, 2 mm \times 2 mm voxel size, 3-mm slice thickness, 130 mm \times 162.5 mm field of view, 90° flip angle). Regions of interest (ROI) were manually defined. T_2 relaxation times were calculated by a linear fit of the logarithmic signal amplitudes versus echo time.

T_1 maps were acquired using a multi-slice, multi-shot, fast-field-echo Look-Locker inversion recovery sequence using simulated electrocardiogram triggering (30 bpm stimulated heart rate, 70-ms phase interval, 6–8 ms TR, 3–4 ms TE, 160×160 reconstruction matrix, 5-mm slice thickness, 170 mm \times 150 mm field of view,

10° flip angle). Relaxation signal amplitudes were fitted to a signal model to yield T_1 relaxation times.

Relaxivities r_1 and r_2 for FLUSPIO and Feraspin XS® were determined by a linear fit of the inverse relaxation times as a function of the iron concentrations.

2.4.6 Time-of-flight secondary ion mass spectrometry (TOF-SIMS)

TOF-SIMS is a high-vacuum surface technique, which provides details about a surface (1–2 nm analysis depth) with high chemical sensitivity (ppm). The surface chemical composition of USPIO and FLUSPIO samples was determined using the Ion ToF IV instrument (ION-TOF GmbH, Münster, Germany). Samples were prepared as described in the AFM section 2.4.1 above.

2.4.7 X-ray photoelectron spectroscopy (XPS)

The quantitative surface elemental composition of USPIO and FLUSPIO samples was determined using a Kratos Axis Ultra XPS instrument (Kratos Axis Ultra, Manchester UK). This technique provides quantitative information from a surface analysis depth of 5–10 nm.

2.4.8 Stability of FLUSPIO in physiological solutions

The colloidal stability of FLUSPIO suspended in different physiologically relevant solutions was checked at different settling times. For our study, we suspended 3.0 $\mu\text{mol Fe/mL}$ FLUSPIO in water, 5% (*w/v*) glucose solution, FCS alone, 1:1 (*v/v*) mixture of 5% glucose solution and FCS, and 25 mM HEPES buffer (pH 7.2), respectively. Subsequently, photographs of the colloidal suspensions were taken at different time points (0, 0.5, 1, 3, 12, and 24 h) using a high-resolution digital camera.

2.5 Cell culture

LnCap cells were procured from American Type Culture Collection (ATCC), USA. Human umbilical vein endothelial cells (HUVEC) were obtained from Promocell GmbH, Heidelberg, Germany. LnCap cells were cultured in RPMI medium with Glutamax (Gibco, Invitrogen, Germany), 20% FCS (Invitrogen, Germany) and 1% Pen/Strep (10,000 U/mL penicillin; 10,000 $\mu\text{g/mL}$ streptomycin, Invitrogen, Germany). HUVEC were grown in human endothelial cell growth medium

(VascuLife VEGF, Lifeline Cell Technology, Troisdorf Germany) containing growth supplements, 2% FCS and 1% Pen/Strep. Cells were cultured in T75 cm^2 cell culture flasks (Cell Star, Greiner, Germany) and incubated at 37 °C under 5% CO_2 and 95% relative humidity conditions until they were confluent.

2.5.1 Cellular viability testing with trypan blue staining

The viability of LnCap cells and HUVEC after incubation with FLUSPIO was evaluated using trypan blue staining (trypan blue solution, Sigma-Aldrich, Steinheim, Germany). Cells (2×10^6) were seeded in 6-well plates (BD Falcon, Germany) and incubated overnight. After incubation, medium was removed and cells were washed with PBS. Cells incubated with cell growth media served as negative controls. The positive controls were generated by exposing the cells to 90 °C for 10 min. Further control groups were maintained under normal growth conditions but after adding the coating molecules FMN and GMP to the growth medium at different concentrations. USPIO and FLUSPIO were diluted in respective cell growth media to 0.03, 0.3, 3.0 $\mu\text{mol Fe/mL}$ and cells were incubated for 3 and 24 h, respectively. Triplicates per condition were analyzed. Subsequently, cells were washed, trypsinized (0.25% trypsin/0.05% EDTA) and centrifuged. Equal amounts of the cell suspension and trypan blue solution were mixed prior to measurement. Trypan blue-positive cells (dead cells) were counted using a Cedex XS cell counter and the percentage of positive cells was reported as a function of the total cell count.

2.6 Competitive binding studies (Prussian blue staining)

To evaluate the specific binding of FLUSPIO to LnCap cells and HUVEC, competitive binding studies were performed. Cells were seeded on glass slides (76 mm \times 26 mm) placed inside a quadriPERM chamber (Greiner, Germany) and incubated overnight to allow them to adhere onto the surface. Prussian blue iron staining was used to visualize FLUSPIO (0.3 $\mu\text{mol Fe/mL}$) uptake and its inhibition after addition of 10- or 100-fold excess of free FMN for 1 h. Additionally, controls were carried along where cells were incubated with cell

growth medium only or with USPIO (0.3 $\mu\text{mol/mL}$). After incubation for 1 or 3 h, cells were washed thrice with PBS and fixed using 4% paraformaldehyde solution. Subsequently, the fixed cells were treated for 5 min with an aqueous solution of $\text{K}_4\text{Fe}(\text{CN})_6$ (10%) and then with a 1:1 mixture of $\text{K}_4\text{Fe}(\text{CN})_6$ (10%) and HCl acid (20%) for 30 min. Subsequently, cells were counterstained with Nuclear Fast Red (Carl Roth, Karlsruhe, Germany). Cover slips were mounted using Mowiol medium and cells were analyzed by bright-field microscopy (Imager M2, Carl Zeiss Microimaging GmbH, Germany) at different magnifications and fields of view.

2.7 MR characterization of competitive binding studies

Specificity of FLUSPIO nanoparticles for Rf receptors expressed in LnCap cells and HUVEC was studied by MRI through competitive-binding studies. Cells were pre-incubated for 10 min with 10-fold excess of free FMN. Consecutively, FLUSPIO (0.3 $\mu\text{mol/mL}$) were added and cells were incubated for 1 h at 37 °C. Cell growth medium, USPIO (0.3 $\mu\text{mol/mL}$) and Feraheme® (0.3 $\mu\text{mol/mL}$) were used in control samples under comparable conditions. Three samples were analyzed per condition. After incubation, cells were washed with saline solution and trypsinized by adding 4 mL trypsin/EDTA (0.25%/0.05%). Trypsinization was stopped by adding respective cell growth media and the cell suspension was centrifuged at 1,000 rpm (Multifuge, Thermo scientific, Germany) for 5 min. The pellet was washed thrice by centrifugation with saline. Cells (0.5×10^6 cells/0.3 mL) were suspended in 10% gelatin and analyzed by MR-relaxometry as described in section 2.4.5.

2.8 MR imaging of FLUSPIO accumulation in LnCap xenografts in mice

All animal experiments were approved by the government review committee on animal care. In this study, LnCap tumor xenografts were chosen since LnCap cells display high expression of RCP [15]. LnCap tumor xenografts were induced by subcutaneous injection of 5×10^6 LnCap cells [21] into the right hind limb of 10 BALB/c male nude mice (Charles River

Laboratories International, Inc., Wilmington, MA, USA). MR investigations were carried out when tumors reached the size of 4 mm \times 4 mm (volume of approximately 33 mm³). The mice ($n = 5$) were then, intravenously injected with 900 $\mu\text{mol Fe/kg}$ FLUSPIO. In the competitive-binding group ($n = 5$), mice were injected with 10-fold excess FMN at 10 min before FLUSPIO (900 $\mu\text{mol Fe/kg}$) administration. MR imaging of LnCap tumor xenografts pre- and post-particle injection (1 and 3 h) was performed under isoflurane anesthesia (2%) using a clinical 3T MRI system (Philips Achieva 3.0 T), in combination with a custom-built small animal solenoid sense-receive mouse coil [17].

To visualize anatomic details, transverse T_2 -weighted MR images of the tumors were acquired using a multi-shot turbo-spin-echo sequence (1,400 ms/100 ms (TR/TE), 0.2 mm \times 0.2 mm voxel size, 1-mm slice thickness, 144 \times 144 reconstruction matrix size, and 25-mm field of view). T_2^* -weighted MR images were acquired using a fast-field-echo sequence (117 ms/26 ms (TR/TE), 0.2 mm \times 0.2 mm voxel size, 1-mm slice thickness, 96 \times 96 reconstruction matrix size, 25-mm field of view and 30° flip angle). Subsequently, T_2^* relaxometry was performed at the same location using a multi-shot, multi-slice fast-field-echo sequence (125 ms/(10–190 ms) TR/TE (TE with 15 different echo times), 0.3 mm \times 0.3 mm voxel size, 1-mm slice thickness, 144 \times 144 reconstruction matrix size, 40-mm field of view, 30° flip angle and 7.9-ms interval between two echoes).

Post-processing was performed on the basis of PAR/REC4 images by applying an IDL (version 6.1)-based software. Subsequently, color-coded R_2^* relaxation rate pixel maps of tumors were generated using the PRIDE analysis software (Philips Healthcare, Germany).

2.9 Immunohistochemistry and bio-distribution

2.9.1 Immunofluorescence of LnCap tumors

LnCap tumor sections (8- μm thickness) were stained for endothelial cells (vessels) by incubation with a primary rat anti-mouse CD31 (PECAM-1) antibody (BD Bioscience, Heidelberg, Germany) for 2 h (room temperature), followed by Cy3-labeled anti-rat IgG secondary antibody (Dianova GmbH, Hamburg, Germany) for 45 min (room temperature). Subsequently, different LnCap tumor sections were stained for

macrophages using a primary rat anti-mouse CD68 antibody (AbD Serotec, Duesseldorf, Germany) for 2 h (room temperature) combined with a Cy3-labeled anti-rat IgG secondary antibody for 45 min (room temperature). Nuclei in the tumor sections were counterstained with DAPI (Merck KGaA, Darmstadt, Germany). Fluorescence microscopy analysis (Imager M2, Carl Zeiss Microimaging GmbH, Germany) was performed at different magnifications (10×, 20×, and 40×) and fields of view.

2.9.2 Combined Prussian blue and hematoxylin-eosin (HE) staining of LnCap tumors

Cryo-preserved (−80 °C) LnCap tumors covered with Tissue-Tek (O.C.T. Compound, Sakura Finetek Europe B.V., Germany) were sectioned and then subjected to combined Prussian blue and HE staining. The Prussian blue staining protocol was performed as described in section 2.6, except that no nuclear fast red staining was performed. Subsequently, the tumor sections were treated with hematoxylin (Carl Roth GmbH, Germany) and with a 1% aqueous solution of eosin (Carl Roth GmbH, Germany). Then, tumor sections were washed with PBS, dehydrated by incubation with an increasing percentage of alcohol (70%, 96%, and 100%) and incubated in xylene. Cover slips were mounted on the sections using Vitro-Clud (R. Langenbrinck, Emmendingen, Germany), a xylene-based mounting medium before microscopic analysis (Imager M2, Carl Zeiss Microimaging GmbH, Germany).

2.9.3 Bio-distribution of FLUSPIO in tumor-bearing mice

For mice ($n = 5$) injected with FLUSPIO, after MRI measurement, liver, spleen, lung, kidney, heart, colon, bladder, muscle, and skin as well as LnCap tumors were excised and subjected to bio-distribution evaluation using an iron-based colorimetric assay. The excised organs and tumors were weighed prior to dissolving them in 3 mL aqua regia by sonication. Subsequently, 1 mL sample solution was diluted in water (1:2 and 1:10) and mixed with phosphate buffer, 4 M NaOH, and 0.25 M Tiron[®]. The absorbance of the iron-tiron complex was measured at 520 nm. Particle-related iron uptake was determined by normalizing the estimated iron contents to organ weights and by subtracting the intrinsic iron content in organs/tumors

derived from mice that were not administered FLUSPIO injections.

2.9.4 Statistics

The differences between groups were tested for statistical significance using a two-tailed, unpaired student's *t*-test considering *p*-values below 0.05 as significant.

3 Results and discussion

3.1 FLUSPIO synthesis

USPIO nanoparticles prepared in water are prone to oxidative degradation at their surface in the absence of a protective coating. In addition, without surface functionalization, USPIO uptake by most tissues and cells is low, except for those of the reticuloendothelial system (RES), which rapidly remove the particles from the blood. Therefore, we selected FMN as a specific, fluorescent, non-polymeric coating molecule, which adsorptively binds to the iron oxide cores via phosphate groups (Fig. 1(a)). Adsorptive fluorescent coating was accomplished by sonication of USPIO and FMN together (pH 4) at ambient temperature. Protecting the surface of USPIO nanoparticles with FMN only led to partial sedimentation of the particles (visual observation) resulting in less-stable suspensions. Therefore, to achieve colloidal stability and sustain FMN fluorescence without quenching under aqueous conditions, the surface of USPIO nanoparticles was additionally covered with non-toxic and biocompatible GMP. We previously demonstrated that a ratio of 0.7:0.3 between GMP and FMN molecules is needed to expedite complete coverage of USPIO nanoparticle surface [17]. Figures S1(a) and S1(b) in the Electronic Supplementary Material (ESM) show a schematic sketch of the adsorptive coating of USPIO using FMN and GMP. Based on the theoretical calculation to achieve a monolayer coating of FMN on the USPIO nanoparticle surface, 0.004 FMN ligands were required per USPIO particle (section S2 in the ESM). In this context, further functionalization of the FLUSPIO can be achieved by linking small molecules (e.g. peptides, therapeutic drugs) either via the free amine at the GMP's guanosine moiety or using suitable spacers (PEG).

3.2 FLUSPIO characterization

The morphology, mean particle size, and size distribution of FLUSPIO were studied using AFM, and DLS techniques. AFM analysis of USPIO showed

particles with spherical morphology with a size range of 10 to 50 nm (Fig. 1(b)), which conforms to previous transmission electron microscopy (TEM)- and scanning electron microscopy (SEM)-based size measurements [17]. Similarly, AFM analysis of FLUSPIO showed

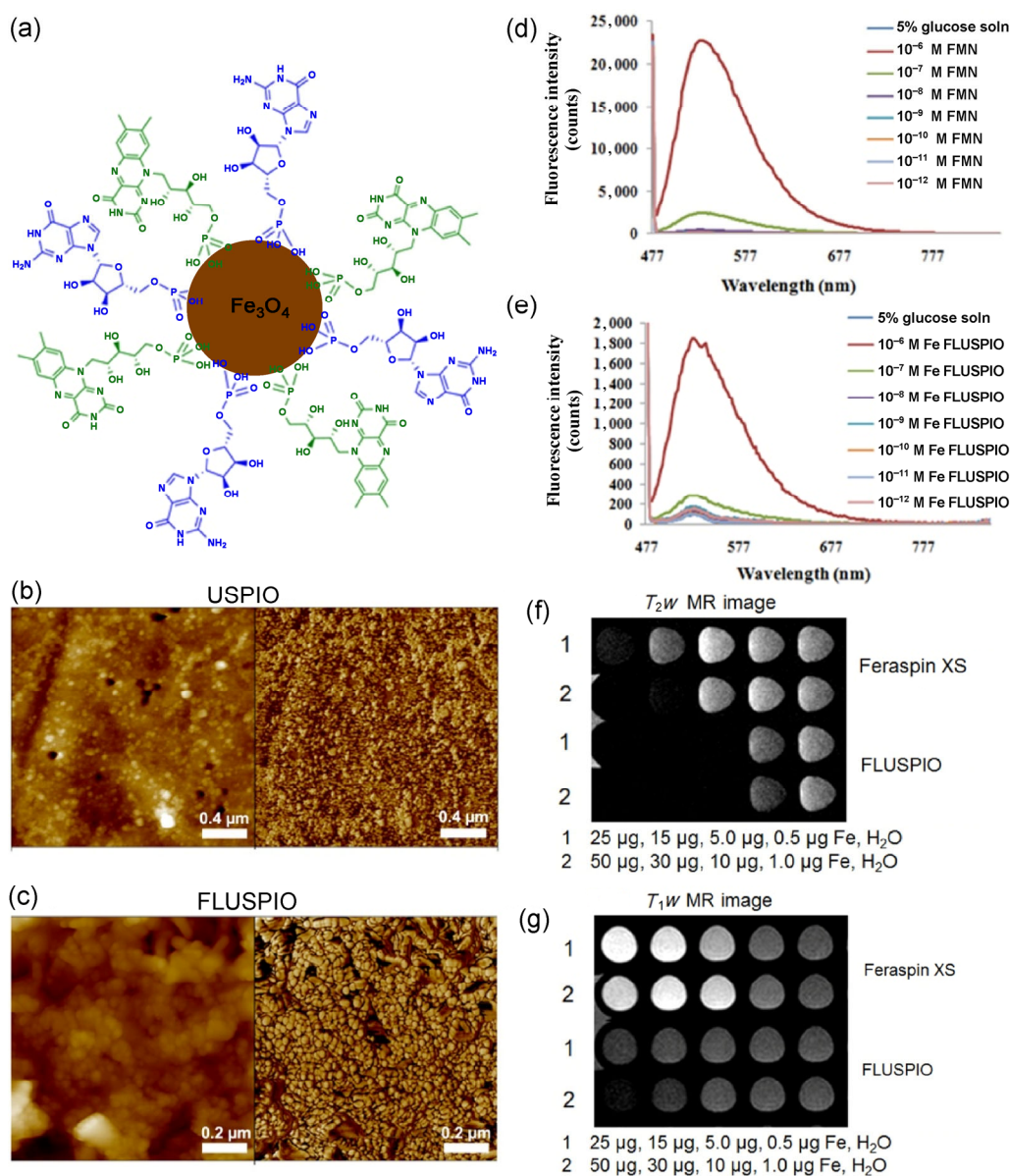


Figure 1 Physical and chemical characterization of FLUSPIO. (a) The schematic diagram illustrates the adsorptive coating of USPIO with FMN and GMP via their phosphate groups. (b) and (c) AFM images of USPIO (b) and FLUSPIO (c) where the topography is shown on the left and phase images on the right. The phase images show spherical surface morphology of FLUSPIO with particles sizes of 20–40 nm. (d) and (e) Fluorescence spectra of FMN (d) and FLUSPIO (e) measured in 5% glucose solution show emission peaks at 530 nm. The observed reduction in fluorescence intensity of FLUSPIO in comparison to FMN can be due to partial FMN quenching and competitive interaction of glucose molecules with USPIO surface. (f) and (g) Contrast enhanced MR images of FLUSPIO compared to commercial iron oxide nanoparticles (Feraspin XS[®], core size of 10–20 nm) at different iron concentrations. (f) T_2W images reveal higher T_2 contrast of FLUSPIO than Feraspin XS[®] in water. (g) In contrast, T_1W images display higher T_1 MR contrast for Feraspin XS[®] than FLUSPIO, which is in line with the manufacturer’s report about its relaxivity.

regions of the sample with defined particulate morphology and size ranging from 20 to 40 nm (Fig. 1(c)), respectively. TEM-based quantitative size analysis of FMN-coated USPIO, achieved after first coating step, revealed similar core sizes (5 ± 1 nm) compared to final FLUSPIO particles (Figs. S2(a) and S2(b) in the ESM).

Nanoparticles are known to interact with plasma proteins in the blood and are subsequently surrounded by a protein corona that significantly alters their size, charge, and biological behavior. The change in size distribution of FLUSPIO nanoparticles after interaction with plasma proteins was investigated by DLS. For this purpose, FLUSPIO nanoparticles were suspended in 10 mM HEPES buffer containing different concentrations (% *w/v*) of HSA. DLS measurements of FLUSPIO in the presence of HSA revealed sizes of 109 ± 6 (0.04% HSA), 107 ± 4 (0.4% HSA), and 134 ± 2 nm (4.0% HSA) with a polydispersity index of 0.31. The size increase of FLUSPIO nanoparticles in presence of 4.0% HSA can be explained by adsorption of plasma proteins [22, 23] forming a protein corona and by non-specific and weak binding of HSA to Rf [24].

Zeta potential measurements were performed to determine the surface charge, electrophoretic mobility, and colloidal stability of USPIO and FLUSPIO in different physiological solutions. USPIO showed negative zeta potentials in FCS, FCS mixed with 5% glucose (1:1) and HEPES buffer, but positive values in 5% glucose solution and water (Table 1). In comparison to USPIO nanoparticles, zeta potentials of FLUSPIO nanoparticles were more negative in all solutions (always < 10). Lowest values were observed in 5% glucose solution, followed by water, HEPES buffer, 5% glucose solution with FCS, and FCS alone, which implies colloidal stability under physiological conditions (Table 1). In this context, the higher zeta potentials in FCS and in the 1:1 mixture of 5% glucose and FCS

indicate some amount of loss in stability due to non-specific protein adsorption as described above. However, it is important to note that binding of soluble RCP to FLUSPIO, may even be beneficial for cellular targeting and uptake [25].

3.3 Fluorescence properties of FLUSPIO

Free FMN suspended in different physiological solutions at varied concentrations revealed intense emission at 530 nm. Highest fluorescence intensity was observed with 5% glucose at 37 °C (Fig. 1(d)) as compared to FCS alone and 5% glucose/FCS (1:1) solutions (Figs. S3(a) and S3(b) in the ESM). The partial reduction of fluorescence in protein solutions could be due to non-specific association between FMN and serum proteins [26].

Surprisingly, in contrast to free FMN, FLUSPIO fluorescence was not affected when suspended in FCS or 5% glucose/FCS (1:1) solution (Fig. 1(e) and Figs. S3(c) and S3(d) in the ESM). This can be related to conformational changes in FMN on the surface of FLUSPIO nanoparticles, reducing non-specific interaction of FMN with FCS. These stable fluorescent properties are highly beneficial, in particular, when considering FLUSPIO for longitudinal cell-labeling studies and for fluorescence-based histological analysis.

3.4 Magnetic properties of FLUSPIO

The MR relaxivity and contrast enhancement properties of FLUSPIO suspended in de-ionized water at different iron concentrations were determined and compared to the commercial MR contrast agent, Feraspin XS[®], which has a similar core size (Figs. 1(f) and 1(g)). FLUSPIO ($r_2 = 368.0 \pm 1.24 \text{ s}^{-1} \cdot \text{mM}^{-1}$) was characterized by a higher T_2 relaxivity than Feraspin XS[®] ($r_2 = 63.06 \pm 0.37 \text{ s}^{-1} \cdot \text{mM}^{-1}$). The higher T_2 relaxivity of FLUSPIO than Feraspin XS[®] can be attributed to the

Table 1 Zeta potentials of USPIO and FLUSPIO suspended in different solutions

| Nanoparticles | Zeta potential (mV) | | | | |
|---------------|---------------------|---------------------------|-------------------|------------------------------------|-------------------|
| | Water | 5% (w/v) glucose solution | FCS | 1:1 (v/v) glucose solution and FCS | HEPES buffer |
| USPIO | 40.70 ± 1.65 | 29.73 ± 1.46 | -6.37 ± 0.29 | -8.57 ± 0.34 | -3.76 ± 0.29 |
| FLUSPIO | -24.23 ± 0.15 | -25.63 ± 0.60 | -10.83 ± 0.25 | -11.03 ± 0.71 | -23.60 ± 2.06 |



formation of nanoclusters during FMN coating, which is reflected by its increased hydrodynamic size. In contrast, the T_1 relaxivity of Feraspin XS[®] ($r_1 = 6.25 \pm 1.41 \text{ s}^{-1} \cdot \text{mM}^{-1}$) was higher than that of FLUSPIO ($r_1 = 3.97 \pm 1.37 \text{ s}^{-1} \cdot \text{mM}^{-1}$), as expected. Therefore, due to high r_2 relaxivity and T_2 contrast enhancement, FLUSPIO may be useful for T_2 -based MR cell labeling, cell tracking, and molecular imaging applications, rather than for T_1 -weighted imaging.

3.5 Chemical composition and colloidal stability of FLUSPIO

The chemical composition of USPIO and FLUSPIO surface was analyzed by TOF-SIMS and XPS techniques. TOF-SIMS provides molecular and chemical information about the outer 1–2 nm of the particle surface. Figures 2(a) and 2(b) compares some key molecular fragments between the USPIO and FLUSPIO

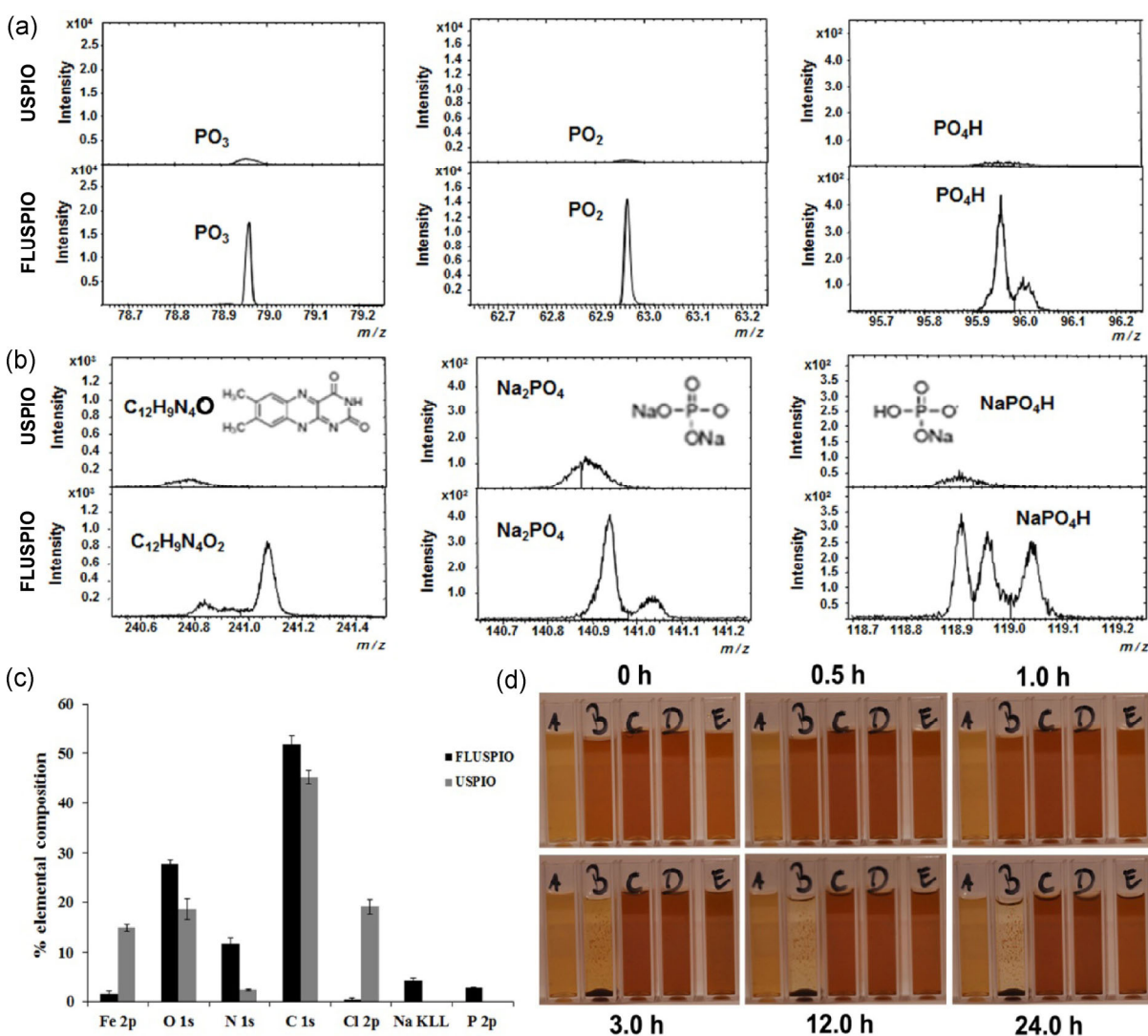


Figure 2 Investigation of surface composition and physiological stability of FLUSPIO in different solutions. (a) and (b) TOF-SIMS spectra of USPIO (a) and FLUSPIO (b) confirm the presence of adsorptive molecules (respective fragmentation peaks) on FLUSPIO surface compared to USPIO displaying no prominent fragmentation peaks. (c) Elemental composition of USPIO and FLUSPIO determined by XPS showed an increase in percentages of carbon, nitrogen, and phosphorous on FLUSPIO surface compared to USPIO, which is in line with the TOF-SIMS data. (d) Digital photographs of FLUSPIO (3.0 $\mu\text{mol Fe/mL}$) suspended in physiological solutions such as H₂O (A), 5% glucose solution (B), FCS alone (C), 1:1 (v/v) mixture of 5% glucose solution and FCS (D), and 25 mM HEPES buffer (pH 7.2) (E), at different settling times (0, 0.5, 1.0, 3.0, 12.0, and 24.0 h), respectively. FLUSPIO exhibited good stability in all solutions for up to 1 h and in all solutions except for 5% glucose, for up to 24 h.

samples. Some peaks are only present in FLUSPIO, which are related to phosphate chemical functionality. The higher mass peaks shown in Fig. 2(b) relate directly to molecular fragments from the coating composition (insert in Fig. 2(b)).

Comparison of the elemental surface composition obtained by XPS measurements (Fig. 2(c)) shows a clear difference between the uncoated USPIO and coated FLUSPIO nanoparticles. The increase in carbon, nitrogen, and phosphorous in FLUSPIO compared to USPIO confirms the successful adsorptive coating with FMN and GMP. Due to the analysis depth of the technique (5–10 nm), there is still a remnant iron signal visible from the FLUSPIO sample (Fig. 2(c)).

The colloidal stability of FLUSPIO (3.0 $\mu\text{mol Fe/mL}$) suspended in various physiological solutions (water, 5% glucose solution, FCS alone, 1:1 mixture of 5% glucose solution and FCS, and HEPES buffer) was visualized through digital photographs at different settling times (0, 0.5, 1, 3, 12, and 24 h) (Fig. 2(d)). The photographs indicate colloidal stability without sedimentation of FLUSPIO except for 5% glucose until 24 h (Fig. 2(d)).

The sedimentation rate in 5% glucose solution was consistent with previous results [17]. Of note, a lower dosage of FLUSPIO (e.g., 0.9 $\mu\text{mol Fe/mL}$) in 5% glucose was used for *in vivo* application in this study and the suspension was immediately injected into the blood.

One of the other physiological solutions evaluated in this study will be selected for further study, via systemic administration of FLUSPIO *in vivo*.

3.6 Cytotoxicity assay

The biocompatibility of FLUSPIO with LnCap cells and HUVEC was evaluated by trypan blue staining. As shown in Figs. S4(a)–S4(d) in the ESM, trypan blue staining indicated no significant reduction in cell viability of both cell types until 24 h, at labeling concentrations of up to 0.3 $\mu\text{mol Fe/mL}$. Consistent with these results, another previous study showed that even high FLUSPIO concentrations do not negatively affect cellular proliferation and integrity or induce major oxidative stress [27].

3.7 Competitive binding studies (Prussian blue staining and MRI)

The cellular uptake of FLUSPIO by prostate cancer (LnCap) and activated endothelial cells (HUVEC) was studied using Prussian blue staining, where internalized FLUSPIO were visible as blue granules in the cytoplasm of the cells. After incubation of LnCap cells with FLUSPIO for 1 h stronger uptake of FLUSPIO (0.3 $\mu\text{mol Fe/mL}$) than USPIO was observed (Fig. 3(a)). HUVEC incubated for 1 h with FLUSPIO showed even higher uptake than LnCap cells (Fig. 3(a)). This trend persisted and was also visible when the incubation time was increased to 3 h (Figs. S5(a)–S5(f) in the ESM). The higher uptake by HUVEC than LnCap cells might be due to cell type-specific characteristics and increased metabolic activity linked to elevated Rf-transporter expression [28]. Thus, we speculate that *in vivo*, FLUSPIO mostly labels the endothelial layer of angiogenic blood vessels prior to their entry into the tumor tissue.

Furthermore, after 1 h of incubation, the competitive inhibition of FLUSPIO uptake by LnCap cells and HUVEC by addition of 10- and 100-fold excess FMN was visualized by Prussian blue staining (Fig. 3(a)) and confirmed their target specificity.

Subsequently, we used MR Relaxometry to quantify the cellular internalization of FLUSPIO and the specificity of its uptake (Fig. 3(b)). For these experiments, LnCap cells were used, which are more uniform and easy to handle than primary cultures of endothelial cells. Furthermore, LnCap cells have been described to display the highest RCP levels among all prostate cancer cells tested so far [15].

After incubation with FLUSPIO, LnCap cells showed a significantly higher R_2 relaxation rate ($11.29 \pm 1.64 \text{ s}^{-1}$, $p < 0.001$) compared to cells incubated with USPIO ($2.88 \pm 0.41 \text{ s}^{-1}$) and Feraheme® ($1.83 \pm 0.26 \text{ s}^{-1}$) indicating higher cellular internalization of FLUSPIO. After adding 10-fold excess of free FMN and subsequent incubation with FLUSPIO for 1 h, the R_2 relaxation rates were significantly lower ($6.38 \pm 0.66 \text{ s}^{-1}$, $p < 0.05$) compared to FLUSPIO alone ($11.29 \pm 1.64 \text{ s}^{-1}$) (Fig. 3(b)). This indicates that the uptake of FLUSPIO is mediated by Rf receptors. We have further

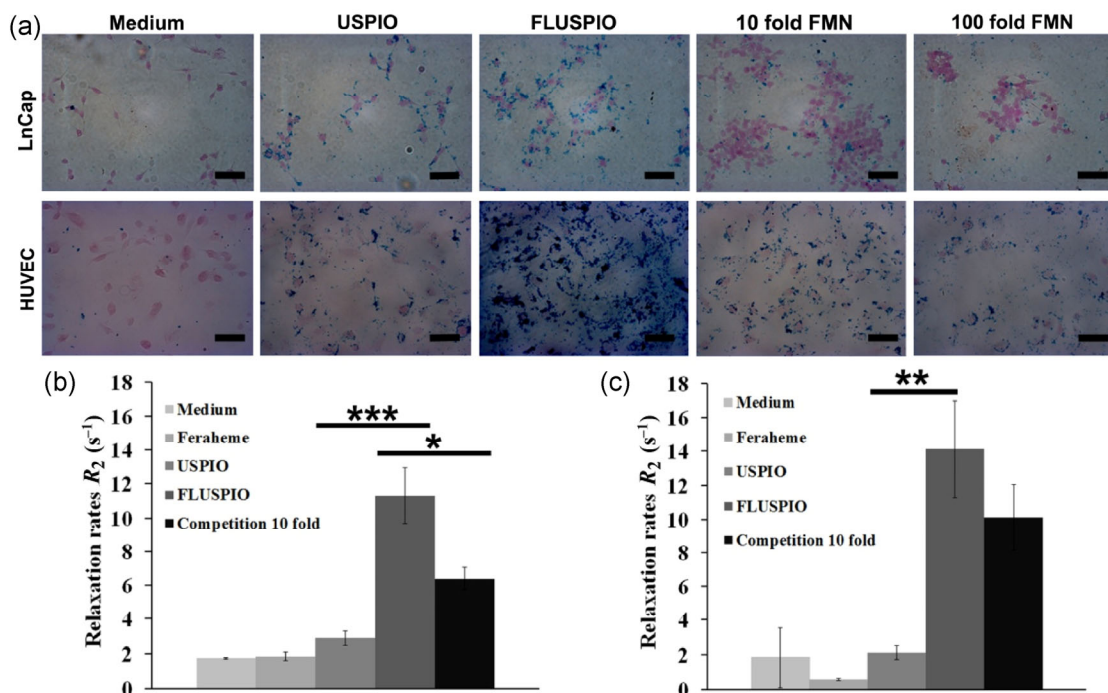


Figure 3 Cellular uptake and specificity of FLUSPIO as studied by Prussian blue staining and MRI. (a)–(c) Prussian blue images of LnCap and HUVEC after 1 h incubation with cell growth media, USPIO (0.3 $\mu\text{mol Fe/mL}$) and 0.3 $\mu\text{mol Fe/mL}$ of FLUSPIO. The uptake of FLUSPIO is visualized by blue granules in the cytoplasm of the cells and higher for FLUSPIO than USPIO in HUVEC and LnCap cells. Furthermore, the uptake of FLUSPIO is higher in HUVEC than in LnCap cells. The specificity of the FLUSPIO for Rf receptors expressed by LnCap cells and HUVEC is indicated by competitively inhibiting their uptake with 10- and 100-fold excess of FMN (a). Scale bar: 50 μm . (b) and (c) Results from MR relaxometry: The uptake of FLUSPIO by LnCap cells (b) and HUVEC (c) was significantly higher (** $p < 0.005$, *** $p < 0.001$) for FLUSPIO than USPIO and Feraheme[®] (all particles: 0.3 $\mu\text{mol Fe/mL}$). The specificity of FLUSPIO uptake is indicated by reduced R_2 relaxation rates after competitively blocking the receptors with 10-fold excess of free FMN (* $p < 0.05$).

validated the specific uptake of FLUSPIO in HUVEC that served as a model of angiogenic endothelium. HUVEC labeled with FLUSPIO displayed significantly higher relaxation rates ($14.15 \pm 2.83 \text{ s}^{-1}$, $p < 0.005$) compared to USPIO ($2.11 \pm 0.39 \text{ s}^{-1}$) and Feraheme[®] ($0.57 \pm 0.06 \text{ s}^{-1}$) (Fig. 3(c)) at incubation conditions analogous to LnCap. In line with the results from histological evaluation, the uptake of FLUSPIO by HUVEC was higher than that by LnCap cells. The uptake of FLUSPIO by HUVEC was also reduced after blocking the receptors with 10-fold excess FMN. The relaxation rate of HUVEC incubated with FLUSPIO was $14.15 \pm 2.83 \text{ s}^{-1}$, whereas with FLUSPIO and FMN, a value of $10.11 \pm 1.96 \text{ s}^{-1}$ was achieved (Fig. 3(c)). Taken together, MR relaxometry results show stronger uptake of FLUSPIO by angiogenic endothelial cells than prostate cancer cells (LnCap), consistent with results from Prussian blue staining.

Although the specificity of uptake was proven for both cell types, the exact uptake mechanism is still unclear. The function of Rf receptors is complex since Rf transporters (RFTs [29–32]) in the cell membrane internalize free Rf as well as the complex of Rf and its carrier protein RCP. There is a hypothesis that uptake of the latter occurs via clathrin-mediated endocytosis, which is one of the fastest and most efficient internalization pathways for nanoparticles [16]. In this context, the impact that RCP and its complexation with FMN on the FLUSPIO nanoparticle surface had on cell uptake is unclear and is part of ongoing research.

3.8 *In vivo* uptake of FLUSPIO nanoparticles

Mice injected with FLUSPIO (900 $\mu\text{mol Fe/kg}$) comprised the specific group ($n = 5$), whereas those injected with 10-fold excess FMN followed by FLUSPIO

comprised the competitive-binding group ($n = 5$). At 1 and 3 h post-intravenous injection of FLUSPIO, a significantly stronger increase in R_2^* relaxation rates was observed in prostate cancer xenografts of the specific than the competitive-binding group (FLUSPIO vs. competition at 1 h: $22.28 \pm 7.22 \text{ s}^{-1}$ versus $6.18 \pm 3.84 \text{ s}^{-1}$, $p < 0.005$; at 3 h: $18.78 \pm 5.80 \text{ s}^{-1}$ versus $7.72 \pm 3.57 \text{ s}^{-1}$, $p < 0.05$) (Fig. 4(g)). These changes in R_2^* relaxation rates are clearly visible in the color-coded R_2^* pixel maps overlaid on T_2^* -weighted images

(Figs. 4(a)–4(f)), proving that the concept of Rf-based tumor targeting with nanoparticles is successful *in vivo*. The chosen experimental time points were early since FLUSPIO nanoparticles display a short circulation time of only 30 min (unpublished data). Thus, the passive accumulation of FLUSPIO via the “Enhanced Permeability and Retention” (EPR) effect is low, which is advantageous for molecular imaging purposes but not optimal to maximize particle accumulation in the tumors, as required for therapeutic nanomedicines.

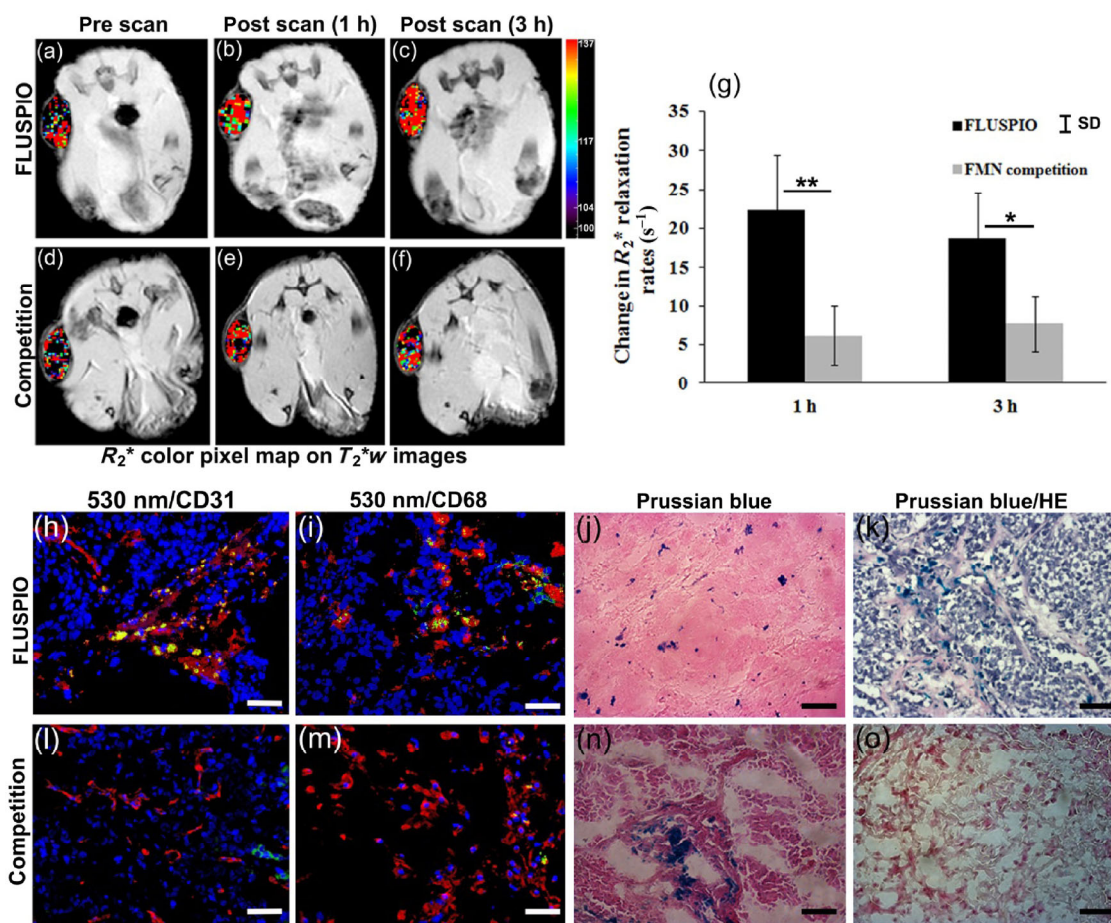


Figure 4 *In vivo* accumulation and competitive binding experiments using LnCap tumor xenografts, as analyzed by MRI and immunohistochemistry. (a)–(f): The R_2^* color-coded pixel maps were overlaid on T_2^* -weighted MR images (transversal slice) of LnCap tumors ($n = 5$) pre- and post-intravenous injection (1 and 3 h) of FLUSPIO ((a)–(c), specific group) and 10-fold FMN + FLUSPIO ((d)–(f), competition group), respectively. The increase in R_2^* relaxation rate after FLUSPIO injection (g) is shown by an increase in red color in the color-coded pixel map ((b) and (c)). Significantly less accumulation (g) is observed in the competitive binding group ((e) and (f)). * $p < 0.05$, ** $p < 0.005$. Triple fluorescence images ((h), (i), (l), and (m)) (cell nuclei, DAPI: blue, endothelial cells, CD31: red, FLUSPIO: green) show highly vascularized tumors and FLUSPIOs’ localization inside (yellow) and outside of the endothelium of tumor blood vessels, which is in line with Prussian blue- (j) and Prussian blue/HE-stained (k) images. The triple fluorescence (l) and Prussian blue/HE-stained images of LnCap tumors from the competitive binding group revealed lower accumulation of FLUSPIO ((n) and (o)). There was also particle uptake by macrophages (red, CD 68) in tumors of the FLUSPIO group (yellow signals in (i)), which was reduced by competitive blocking (m). Together, these results clearly show accumulation of FLUSPIO nanoparticles in endothelial cells, tumor associated macrophages, and tumor cells as well as their *in vivo* specificity for RCP. Scale bar: 50 μm .

For this purpose FLUSPIO will need modifications using appropriate ligands (e.g. PEG).

3.9 Immunohistological assessment of *in vivo* accumulation of FLUSPIOs

LnCap tumor sections derived from the FLUSPIO and competitive-binding groups were used for immunofluorescence (IF) and histology-based validation of MR findings. Tumor vessels were stained for CD31 (red) and nuclei were counter-stained with DAPI (blue). Triple-fluorescence images of the LnCap tumor sections show localization of FLUSPIO (green) (Fig. 4(h)) predominantly inside the endothelium but also outside of the angiogenic blood vessel (Fig. 4(h)). IF images of the competitive-binding group show significantly less FLUSPIO accumulation in the tumors, indicating that the particle accumulation is not just related to the EPR effect (Fig. 4(l)). Prussian blue images are consistent with IF images and additionally indicate that entire FLUSPIO nanoparticles and not just desorbed FMN or USPIO were accumulated in the tumors (Figs. 4(j), (k), (n), and (o)).

To further investigate distribution of FLUSPIO inside the tumors, macrophages were stained using an anti-CD68 antibody. Triple fluorescence images of FLUSPIO, cell nuclei, and macrophages indicated FLUSPIO uptake by tumor-resident macrophages (red) (Fig. 4(i)). Since FLUSPIO uptake by macrophages was lower in the competitive-binding group (Fig. 4(m)), uptake by macrophages seems to depend—at least partially—on Rf receptors and not just on unspecific phagocytic activity.

3.10 Bio-distribution of FLUSPIO

As anticipated from previous studies on USPIO bio-distribution, there was a strong uptake of FLUSPIO by organs of the reticuloendothelial systems, in particular the liver and spleen [33, 34]. Further, its accumulation in the lung can be explained by macrophage uptake. The signals in kidney and bladder may derive from a fraction of very small particles (<5 nm) or iron remnants that are small enough to be filtrated. The presence of particles in the colon is the consequence of the mainly hepatobiliary elimination. High accumulation of Rf-receptor targeted particles in the skin was found for

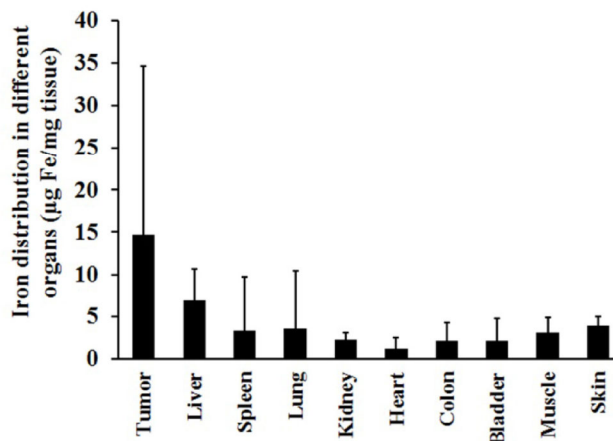


Figure 5 Bio-distribution of FLUSPIO in LnCap tumor xenografts as evaluated by iron colorimetry.

all Rf-based probes that we tested so far and is most probably related to the known high expression of Rf receptors in this organ [35]. Thus, targeting this organ can be considered as a further indication for RFT-targeted nanoparticles and drugs. On the other hand, in safety evaluations of RFT-targeted probes particular care has to be taken not to oversee adverse side effects in the skin. The strong accumulation in the tumor can be explained by FLUSPIO binding to tumor cells, which highly express Rf-receptors and by the binding of FLUSPIO to the cancer related stromal cells, in particular to the endothelial cells and to the tumor macrophages.

4 Conclusions

In summary, we showed that Rf receptor-mediated targeting is an efficient way to accumulate nanoparticles in prostate cancer cells. High levels of FLUSPIO accumulation in the tumors can be explained by its ability to target both, the tumor cell and the stromal compartment, of macrophages and angiogenic endothelial cells. Furthermore, our bio-distribution data indicate that besides the expected nanoparticle uptake by organs of the RES, the skin shows enhanced accumulation that can be related to high Rf receptor expression. Nevertheless, further and more detailed studies will be required to better understand the regulation of the Rf receptor expression in healthy and pathologically altered tissues before it can be considered as a target for diagnostic and therapeutic

probes. In this context, motivated by our results with FLUSPIO, an investigation of other flavin-tagged carrier systems (e.g. liposomes and polymers) for diagnostic, therapeutic, and theranostic applications is underway.

Acknowledgements

This work was supported by the Deutsche Forschungsgemeinschaft (DFG) grant KI 1072/1-3 “Dual modal contrast agents for MRI and optical imaging techniques” by the Helmholtz-Society Portfolio grant “Technologie und Medizin – Multimodale Bildgebung zur Aufklärung des *In-vivo*-Verhaltens von polymeren Biomaterialien”. The authors would like to thank Mr. Yang Shi, department of pharmaceutical science, Universiteit Utrecht, The Netherlands for performing zeta potential measurements and Dr. David Scurr, School of Pharmacy, University of Nottingham, UK for carrying out TOF-SIMS measurements. The authors would like to thank Prof. Dr. Twan Lammers for reading the manuscript.

Electronic Supplementary Material: Supplementary material (details of FLUSPIO synthesis schematics, theoretical prediction of FMN per USPIO, TEM images, fluorescence spectroscopy, cytotoxicity and cellular labeling of FLUSPIO) is available in the online version of this article at <http://dx.doi.org/10.1007/s12274-016-1028-7>.

Open Access: This article is distributed under the terms of the Creative Commons Attribution 4.0 International License (<http://creativecommons.org/licenses/by/4.0/>), which permits unrestricted use, distribution, and reproduction in any medium, provided you give appropriate credit to the original author(s) and the source, provide a link to the Creative Commons license, and indicate if changes were made.

References

- [1] Mamede, A. C.; Tavares, S. D.; Abrantes, A. M.; Trindade, J.; Maia, J. M.; Botelho, M. F. The role of vitamins in cancer: A review. *Nutr. Cancer* **2011**, *63*, 479–494.
- [2] Russell-Jones, G.; McTavish, K.; McEwan, J.; Rice, J.; Nowotnik, D. Vitamin-mediated targeting as a potential mechanism to increase drug uptake by tumours. *J. Inorg. Biochem.* **2004**, *98*, 1625–1633.
- [3] Giancaspero, T. A.; Busco, G.; Panebianco, C.; Carmone, C.; Miccolis, A.; Liuzzi, G. M.; Colella, M.; Barile, M. FAD synthesis and degradation in the nucleus create a local flavin cofactor pool. *J. Biol. Chem.* **2013**, *288*, 29069–29080.
- [4] Becker, K.; Schirmer, M.; Kanzok, S.; Schirmer, R. H. Flavins and flavoenzymes in diagnosis and therapy. In *Flavoprotein Protocols*; Chapman, S. K.; Reid, G. A., Eds.; Humana Press: Totowa, N.J., 1999; pp 229–245.
- [5] Rao, P. N.; Levine, E.; Myers, M. O.; Prakash, V.; Watson, J.; Stoller, A.; Kopicko, J. J.; Kissinger, P.; Raj, S. G.; Raj, M. H. Elevation of serum riboflavin carrier protein in breast cancer. *Cancer Epidemiol. Biomarkers Prev.* **1999**, *8*, 985–990.
- [6] Bareford, L. M.; Swaan, P. W. Endocytic mechanisms for targeted drug delivery. *Adv. Drug Deliv. Rev.* **2007**, *59*, 748–758.
- [7] Bareford, L. M.; Avaritt, B. R.; Ghandehari, H.; Nan, A.; Swaan, P. W. Riboflavin-targeted polymer conjugates for breast tumor delivery. *Pharm. Res.* **2013**, *30*, 1799–1812.
- [8] Huang, S. N.; Phelps, M. A.; Swaan, P. W. Involvement of endocytic organelles in the subcellular trafficking and localization of riboflavin. *J. Pharmacol. Exp. Ther.* **2003**, *306*, 681–687.
- [9] Pedrolli, D. B.; Jankowitsch, F.; Schwarz, J.; Langer, S.; Nakanishi, S.; Frei, E.; Mack, M. Riboflavin analogs as anti-infectives: Occurrence, mode of action, metabolism and resistance. *Curr. Pharm. Des.* **2013**, *19*, 2552–2560.
- [10] Chen, C.; Ke, J. Y.; Zhou, X. E.; Yi, W.; Brunzelle, J. S.; Li, J.; Yong, E. L.; Xu, H. E.; Melcher, K. Structural basis for molecular recognition of folic acid by folate receptors. *Nature* **2013**, *500*, 486–489.
- [11] Wang, S. S.; Low, P. S. Folate-mediated targeting of antineoplastic drugs, imaging agents, and nucleic acids to cancer cells. *J. Control. Release* **1998**, *53*, 39–48.
- [12] Bae, Y.; Jang, W. D.; Nishiyama, N.; Fukushima, S.; Kataoka, K. Multifunctional polymeric micelles with folate-mediated cancer cell targeting and pH-triggered drug releasing properties for active intracellular drug delivery. *Mol. Biosyst.* **2005**, *1*, 242–250.
- [13] D’Souza, V. M.; Foraker, A. B.; Free, R. B.; Ray, A.; Shapiro, P. S.; Swaan, P. W. cAMP-coupled riboflavin trafficking in placental trophoblasts: A dynamic and ordered process. *Biochemistry* **2006**, *45*, 6095–6104.
- [14] Barile, M.; Giancaspero, T. A.; Brizio, C.; Panebianco, C.; Indiveri, C.; Galluccio, M.; Vergani, L.; Eberini, I.; Gianazza, E. Biosynthesis of flavin cofactors in man: Implications in health and disease. *Curr. Pharm. Des.* **2013**, *19*, 2649–2675.
- [15] Johnson, T.; Ouhit, A.; Gaur, R.; Fernando, A.; Schwarzenberger, P.; Su, J.; Ismail, M. F.; El-Sayyad, H. I.; Karande,

- A.; Elmageed, Z. A. et al. Biochemical characterization of riboflavin carrier protein (RCP) in prostate cancer. *Front. Biosci. (Landmark Ed.)* **2009**, *14*, 3634–3640.
- [16] Bareford, L. M.; Phelps, M. A.; Foraker, A. B.; Swaan, P. W. Intracellular processing of riboflavin in human breast cancer cells. *Mol. Pharm.* **2008**, *5*, 839–848.
- [17] Jayapaul, J.; Hodenius, M.; Arns, S.; Lederle, W.; Lammers, T.; Comba, P.; Kiessling, F.; Gaetjens, J. FMN-coated fluorescent iron oxide nanoparticles for RCP-mediated targeting and labeling of metabolically active cancer and endothelial cells. *Biomaterials* **2011**, *32*, 5863–5871.
- [18] Jayapaul, J.; Arns, S.; Lederle, W.; Lammers, T.; Comba, P.; Gätjens, J.; Kiessling, F. Riboflavin carrier protein-targeted fluorescent USPIO for the assessment of vascular metabolism in tumors. *Biomaterials* **2012**, *33*, 8822–8829.
- [19] Jander, G.; Jahr, K.-F. *Massanalyse*. 17 ed.; 2009.
- [20] Bashir, W. A. Photometric determination of iron (III). *Microchem. J.* **1981**, *26*, 477–480.
- [21] Pillarsetty, N.; Punzalan, B.; Larson, S. M. 2-¹⁸F-Fluoropropionic acid as a PET imaging agent for prostate cancer. *J. Nucl. Med.* **2009**, *50*, 1709–1714.
- [22] Jansch, M.; Stumpf, P.; Graf, C.; Rühl, E.; Müller, R. H. Adsorption kinetics of plasma proteins on ultrasmall superparamagnetic iron oxide (USPIO) nanoparticles. *Int. J. Pharm.* **2012**, *428*, 125–133.
- [23] Mahmoudi, M.; Lynch, I.; Ejtehadi, M. R.; Monopoli, M. P.; Bombelli, F. B.; Laurent, S. Protein–nanoparticle interactions: Opportunities and challenges. *Chem. Rev.* **2011**, *111*, 5610–5637.
- [24] Memarpoor-Yazdi, M.; Mahaki, H. Probing the interaction of human serum albumin with vitamin B2 (riboflavin) and l-arginine (l-Arg) using multi-spectroscopic, molecular modeling and zeta potential techniques. *J. Lumin.* **2013**, *136*, 150–159.
- [25] Mason, C. W.; D'Souza, V. M.; Bareford, L. M.; Phelps, M. A.; Ray, A.; Swaan, P. W. Recognition, cointernalization, and recycling of an avian riboflavin carrier protein in human placental trophoblasts. *J. Pharmacol. Exp. Ther.* **2006**, *317*, 465–472.
- [26] Innis, W. S. A.; McCormick, D. B.; Merrill, A. H., Jr. Variations in riboflavin binding by human plasma: Identification of immunoglobulins as the major proteins responsible. *Biochem. Med.* **1985**, *34*, 151–165.
- [27] Mertens, M. E.; Frese, J.; Bölükbas, D. A.; Hrdlicka, L.; Golombek, S.; Koch, S.; Mela, P.; Jockenhövel, S.; Kiessling, F.; Lammers, T. FMN-coated fluorescent USPIO for cell labeling and non-invasive MR imaging in tissue engineering. *Theranostics* **2014**, *4*, 1002–1013.
- [28] Paik, J.-Y.; Lee, K.-H.; Ko, B.-H.; Choe, Y. S.; Choi, Y.; Kim, B.-T. Nitric oxide stimulates ¹⁸F-FDG uptake in human endothelial cells through increased hexokinase activity and GLUT1 expression. *J. Nucl. Med.* **2005**, *46*, 365–370.
- [29] Yonezawa, A.; Masuda, S.; Katsura, T.; Inui, K.-I. Identification and functional characterization of a novel human and rat riboflavin transporter, RFT1. *Am. J. Physiol. Cell Physiol.* **2008**, *295*, C632–C641.
- [30] Yamamoto, S.; Inoue, K.; Ohta, K.-Y.; Fukatsu, R.; Maeda, J.-Y.; Yoshida, Y.; Yuasa, H. Identification and functional characterization of rat riboflavin transporter 2. *J. Biochem.* **2009**, *145*, 437–443.
- [31] Subramanian, V. S.; Subramanya, S. B.; Rapp, L.; Marchant, J. S.; Ma, T. Y.; Said, H. M. Differential expression of human riboflavin transporters -1, -2, and -3 in polarized epithelia: A key role for hRFT-2 in intestinal riboflavin uptake. *Biochim. Biophys. Acta* **2011**, *1808*, 3016–3021.
- [32] Yao, Y.; Yonezawa, A.; Yoshimatsu, H.; Masuda, S.; Katsura, T.; Inui, K.-I. Identification and comparative functional characterization of a new human riboflavin transporter hRFT3 expressed in the brain. *J. Nutr.* **2010**, *140*, 1220–1226.
- [33] Shانهsazzadeh, S.; Oghabian, M. A.; Daha, F. J.; Amanlou, M.; Allen, B. J. Biodistribution of ultra small superparamagnetic iron oxide nanoparticles in BALB mice. *J. Radioanal. Nucl. Chem.* **2013**, *295*, 1517–1523.
- [34] Shانهsazzadeh, S.; Oghabian, M. A.; Allen, B. J.; Amanlou, M.; Masoudi, A.; Daha, F. J. Evaluating the effect of ultrasmall superparamagnetic iron oxide nanoparticles for a long-term magnetic cell labeling. *J. Med. Phys.* **2013**, *38*, 34–40.
- [35] Foraker, A. B.; Khantwal, C. M.; Swaan, P. W. Current perspectives on the cellular uptake and trafficking of riboflavin. *Adv. Drug Deliv. Rev.* **2003**, *55*, 1467–1483.